

LETTER TO THE EDITOR

Detection of extragalactic magnetic massive stars

S. Hubrig¹, M. Schöller², S. P. Järvinen¹, A. Cikota³, M. Abdul-Masih^{4,5},
A. Escorza^{4,5}, and R. Jayaraman⁶

¹ Leibniz-Institut für Astrophysik Potsdam (AIP), An der Sternwarte 16, 14482 Potsdam, Germany
e-mail: shubrig@aip.de

² European Southern Observatory, Karl-Schwarzschild-Str. 2, 85748 Garching, Germany

³ Gemini Observatory/NSF's NOIRLab, Casilla 603, La Serena, Chile

⁴ Instituto de Astrofísica de Canarias, C. Vía Láctea s/n, 38205 La Laguna, Santa Cruz de Tenerife, Spain

⁵ Dpto. Astrofísica, Universidad de La Laguna, Av. Astrofísico Francisco Sánchez, 38206 La Laguna, Santa Cruz de Tenerife, Spain

⁶ MIT Kavli Institute and Department of Physics, 77 Massachusetts Avenue, Cambridge, MA 02139, USA

Received 29 February 2024 / Accepted 26 April 2024

ABSTRACT

Context. Studies of the magnetic characteristics of massive stars have recently received significant attention because they are progenitors of highly magnetised compact objects. Stars initially more massive than about $8 M_{\odot}$ leave behind neutron stars and black holes by the end of their evolution. The merging of binary compact remnant systems produces astrophysical transients detectable by gravitational wave observatories. Studies of magnetic fields in massive stars with low metallicities are of particular interest because they provide important information on the role of magnetic fields in the star formation of the early Universe.

Aims. While several detections of massive Galactic magnetic stars have been reported in the last few decades, the impact of a low-metallicity environment on the occurrence and strength of stellar magnetic fields has not yet been explored. Because of the similarity between Of?p stars in the Magellanic Clouds (MCs) and Galactic magnetic Of?p stars, which possess globally organised magnetic fields, we searched for magnetic fields in Of?p stars in the MCs. Additionally, we observed the massive contact binary Cl* NGC 346 SSN7 in the Small Magellanic Cloud to test the theoretical scenario that the origin of magnetic fields involves a merger event or a common envelope evolution.

Methods. We obtained and analysed measurements of the magnetic field in four massive Of?p stars in the MCs and the binary Cl* NGC 346 SSN7 using the ESO/VLT FORS2 spectrograph in spectropolarimetric mode.

Results. We detected kilogauss-scale magnetic fields in two Of?p-type stars and in the contact binary Cl* NGC 346 SSN7. These results suggest that the impact of low metallicity on the occurrence and strength of magnetic fields in massive stars is low. However, because the explored stellar sample is very small, additional observations of massive stars in the MCs are necessary.

Key words. binaries: spectroscopic – stars: magnetic field – stars: massive – stars: oscillations – stars: variables: general

1. Introduction

The discovery of gravitational wave transients in high-redshift galaxies caused by mergers of black holes and neutron stars in binary systems has radically changed astronomical research, with focus now on advancing our understanding of the life cycle of massive binary and multiple systems. Importantly, magnetism is considered to be a key component in massive star evolution, with a far-reaching impact on their ultimate fate. Highly magnetised neutron stars with very strong magnetic fields, the magnetars, are highly relevant in the field of gravitational wave astronomy (e.g. Regimbau & de Freitas Pacheco 2006). A magnetic mechanism for the collimated explosion of massive stars, relevant for long-duration gamma-ray bursts, X-ray flashes, and asymmetric core collapse supernovae, was proposed in several theoretical studies (e.g. Uzdensky & MacFadyen 2006). Such energetic physical processes affect the structure of entire galaxies and chemically enrich the interstellar medium.

Magnetic massive stars are unique sites to observe the combined effect of stellar winds, rotation, and magnetism. In particular, studies of massive stars with low metallicities are of primary

interest because these stars are especially valuable proxies of the early Universe and of contemporary star-forming galaxies. With low metallicities, massive stars are hotter and more luminous than their metallic counterparts, and their radii are smaller. Furthermore, they have very different wind characteristics, which play a dominant role in the evolution of massive stars (Ekström et al. 2019). Yet, the impact of lower metallicities on the occurrence and strength of stellar magnetic fields in massive stars has not been explored, neither theoretically nor observationally.

The previously reported incidence rate of stable, predominantly dipolar magnetic fields in Galactic O stars, with field strengths in the range from hundreds of gauss to tens of kilogauss, was about 7% (e.g. Grunhut et al. 2017; Schöller et al. 2017). More recently, it was reported that massive stars in binary and multiple systems are more likely to possess magnetic fields (Hubrig et al. 2023). The origin of the magnetic fields in massive stars is still under debate: it has been argued that magnetic fields could be fossils, generated by dynamos, or generated by a strong binary interaction (i.e. in stellar mergers, during a mass transfer, or during a common envelope evolutionary phase). Recent

theoretical research shows that protostellar mergers might offer a tentative explanation for surface magnetic fields in massive stars (Schneider et al. 2019, 2020).

A fraction of the known Galactic magnetic O-type stars belong to the rare class of Of?p-type stars. Of?p stars are identified by the presence of C III 4650 Å emission that is in comparable strength to the neighbouring N III 4634 and 4642 Å lines and recurrent spectral variability, notably in their Balmer and He lines (Walborn 1972). Five Galactic Of?p stars are currently known: HD 108, NGC 1624-2, CPD-28° 2561, HD 148937, and HD 191612 (Walborn et al. 2010), and all of them show evidence of the presence of magnetic fields (Hubrig et al. 2008, 2011; Grunhut et al. 2017). Obviously, the detection of magnetic fields in all five Galactic Of?p stars implies a tight relation between the spectral characteristics of the Of?p star group and the presence of a magnetic field.

The origin of Of?p stars and why only five Galactic stars with this classification have been identified so far is, however, not understood. A useful hint came from the combination of ten years of spectroscopic and interferometric data for the Of?p binary HD 148937, which has an orbital period of 29 yr (Frost et al. 2021). It was concluded that the magnetic primary, although more massive, appears younger, suggesting that a merger or mass transfer took place in this system.

Importantly, massive stars with the Of?p classification have also been identified in the Small and Large Magellanic Clouds (SMC and LMC): three stars each in the SMC (SMC 159-2, OGLE SMC-SC6 237339, and AzV 220) and the LMC (BI 57, LMC 64-2, and UCAC4 115-008604) (e.g. Walborn et al. 2015; Neugent et al. 2018). The SMC and LMC are known to have significantly lower metallicities compared to our Galaxy, $Z_{\text{SMC}} = 0.2 Z_{\odot}$ and $Z_{\text{LMC}} = 0.5 Z_{\odot}$, respectively, and can therefore be used as close proxies for the early Universe. Evidently, due to the similarity with the well-studied Galactic magnetic Of?p stars that possess globally organised magnetic fields, the Of?p stars in the Magellanic Clouds (MCs) can be regarded as the best candidate extragalactic magnetic O-type stars. Therefore, to investigate the impact of low metallicities on the presence and strength of stellar magnetic fields, we applied for observing time with the ESO/VLT Focal Reducer low dispersion Spectrograph (FOR2; Appenzeller et al. 1998) in spectropolarimetric mode. Further, to test theoretical scenarios that suggest that the origin of magnetic fields in massive stars involves a strong binary interaction (e.g. Schneider et al. 2016; Pelisoli et al. 2022), we included in our target list the ON3 If+O5.5 V((f)) contact system Cl* NGC 346 SSN 7 (SSN 7 henceforth), located within the core of the most massive star-forming region in the SMC, NGC 346 (Dufton et al. 2019). NGC 346 is usually considered a counterpart of 30 Doradus in the LMC, and observations of this cluster are frequently used to study the violent feedback effects of massive stars on the formation and evolution of protostars. SSN 7 was recently characterised as a short-period (~ 3.07 d) contact binary by Rickard & Pauli (2023).

In Sect. 2 we describe the obtained observations and their reduction, and we present the measurement procedure in Sect. 3. In Sect. 4 we discuss the results of the magnetic field measurements.

2. Observations and data reduction

Two nights were allocated for our observing programme, which was carried out in visitor mode on 2023 October 3 and 4 using the ESO/VLT FOR2 instrument (Appenzeller et al. 1998), which is capable of imaging, polarimetry, long-slit, and

multi-object spectroscopy. FOR2 is equipped with polarisation analysing optics, comprising super-achromatic halfwave and quarterwave phase retarder plates, and a Wollaston prism with a beam divergence of 22'' in standard resolution mode. As we did not know beforehand exactly when our visitor programme would be scheduled, for the observations of the mean longitudinal magnetic field we selected the four Of?p stars with the longest rotation periods, OGLE SMC-SC6 2373392 (= 2dFS936), BI 57, AzV 220, and UCAC4 115-008604 (= LMCe 136-1), which have periods of 1370 d, 787 d, >16 yr, and 18.7 d, respectively (Bagnulo et al. 2017, 2020). Because the maximum of the longitudinal magnetic field in Galactic massive stars usually occurs at the same time as the maximum of the light curve (Munoz et al. 2020), the idea behind such a selection was to avoid FOR2 spectropolarimetric observations at unfavourable rotation phases when the light curve is at its minimum. For SSN 7, however, the rotation periods of both components are unknown. Rotational phases are particularly important in longitudinal magnetic field measurements since this field component is defined as the component of the magnetic field averaged over the visible stellar disc. Hence, the ability to detect longitudinal magnetic fields critically depends not only on the intrinsic strength of the magnetic field but also on the geometrical view of the stellar magnetic field structure at the time of the observation. To verify the performance of the FOR2 Zeeman analyser, we observed in addition two Galactic targets: the B0.7 IV ξ^1 CMa (= HD 46328), with a magnetic field of the order of a few hundred gauss (Hubrig et al. 2006), and the O4 If+O5-6 system HD 45166, with a kilogauss-scale field (Shenar et al. 2023). We observed each target once.

We used GRISM 600B and a slit width of 0.5'' to achieve a spectral resolving power of about 1650. This instrumental configuration allowed us to cover a larger wavelength range, from 3250 to 6215 Å, which includes all Balmer lines except H α . The detector was a 2k \times 4k MIT CCD with a pixel size of 15 $\mu\text{m} \times$ 15 μm . The MIT CCD has a nominal gain of 1.25 and a readout noise of 2.70 electrons. To minimise the crosstalk effect, the position angle of the retarder waveplate was changed from +45° to -45° and vice versa every second exposure (Hubrig et al. 2004a,b). We executed the sequence -45°, +45°, +45°, -45° twice to increase the final signal-to-noise ratio (S/N). The exposure times ranged from 2.7 h for the brightest Of?p star in the sample, BI 57, with $m_V = 14.0$, to about 4.0 h for the Of?p star AzV 220 with $m_V = 14.5$. The weather conditions were mediocre on our first visitor night, with a seeing of up to 2.1'' and strong winds. This explains the rather low S/N of 680 achieved for the target BI 57. The second night was better, with seeing around 1.2''. Our observation of OGLE SMC-SC6 237339 took place at the rotation phase $\phi = 0.545$, close to the maximum of the Optical Gravitational Lensing Experiment (OGLE) light curve ($\phi = 0.5$). The same is also true for the observations of UCAC4 115-008604 at $\phi = 0.296$, which is close to the light curve maximum ($\phi = 0.4$). Only for the target BI 57 was our observation obtained at a phase between maximum and minimum light, $\phi = 0.250$. The rotation phase of our observation of AzV 220 is unknown due to missing information on its rotation period.

The obtained data were reduced in two ways using a set of completely independent tools and routines. First, from the raw FOR2 data, the spectra recorded in left- and right-hand polarised light (i.e. the ordinary and extraordinary beams) were extracted using a pipeline written in the MIDAS environment (henceforth the MIDAS pipeline). A description of the assessment of the longitudinal magnetic field measurements using

Table 1. Logbook of our observations.

Object	m_V	Spectral Type	Date	MJD	DIT [s]	S/N	Wavelength [Å]
OGLE SMC-SC6 237339	14.0	O6.5?p	2023-10-03	60220.0931	12 500	970	4600
BI 57	14.0	O8?p	2023-10-03	60220.2334	9600	680	4600
AzV 220	14.5	O6.5?p	2023-10-04	60221.0657	14 400	910	4600
UCAC4 115-008604	14.7	O6.5?p	2023-10-04	60221.2405	12 900	720	4220
C1 *NGC 346 SSN 7	12.6	ON3 If+O5.5 V((f))	2023-10-04	60221.3532	4200	1340	4730
ξ^1 CMa	4.3	B0.7 IV	2023-10-03	60220.3053	32	3700	4530
HD 45166	9.9	WRpec+B7 V	2023-10-04	60221.3993	90	860	4600

Notes. Col. 1 gives the object name, followed by the visual magnitude (m_V) and the spectral type in Cols. 2 and 3. In Cols. 4 and 5, we list the date of the observation and the corresponding modified Julian date (MJD). Finally, Col. 6 shows the detector integration time (DIT) and Cols. 7 and 8 the peak S/N values per Å at the wavelengths corresponding to the maximum of the flux distribution for each target.

FORS1/2 spectropolarimetric observations was presented in our previous work (Hubrig et al. 2004a,b). The MIDAS pipeline reduction by default includes sky background subtraction. The wavelength calibration was carried out using He-Ne-Ar arc lamp exposures. A unique wavelength calibration frame was used for each night. The effects of improper flat field correction in the presence of polarisation optics were minimised by taking advantage of the redundant number of quarterwave positions (see Sect. 4.6.1 in the FORS2 User Manual).

The second reduction was performed using standard Image Reduction and Analysis Facility (IRAF¹; Tody 1993) procedures (Cikota et al. 2017). After bias subtraction, the extraction of the spectra corresponding to ordinary and extraordinary beams was carried out in an unsupervised way using the PYRAF apextract.apall procedure, with a fixed aperture size of 50 pixels. IRAF’s apall function was applied to subtract the sky background using small apertures above and below the spectra. To avoid spectrum-tracing problems, the input frames were properly trimmed to exclude the low S/N at the edges of the spectral range. Since the exposure times were relatively long, the polarimetric spectra are affected by cosmics. They were removed using L.A.Cosmic (Laplacian Cosmic Ray Identification; van Dokkum 2001). We did not detect any differences between the spectra extracted using the MIDAS pipeline and those from the IRAF procedures.

For each target, the information on the time of observation, the length of the exposure, and the achieved S/N is presented in Table 1.

3. Measurement procedure

The mean longitudinal magnetic field was determined from the FORS2 observations as the slope of a weighted linear regression through the measured Stokes V values. The linear regression method uses a technique similar to that developed earlier by Angel & Landstreet (1970) and is based on the measurement of the difference between the circular polarisation observed in the red and blue wings of spectral lines. The V/I spectrum was calculated as

$$\frac{V}{I} = \frac{1}{2} \left\{ \left(\frac{f^o - f^e}{f^o + f^e} \right)_{-45^\circ} - \left(\frac{f^o - f^e}{f^o + f^e} \right)_{+45^\circ} \right\}, \quad (1)$$

where $+45^\circ$ and -45° indicate the position angle of the retarder waveplate, and f^o and f^e are the ordinary and extraordinary

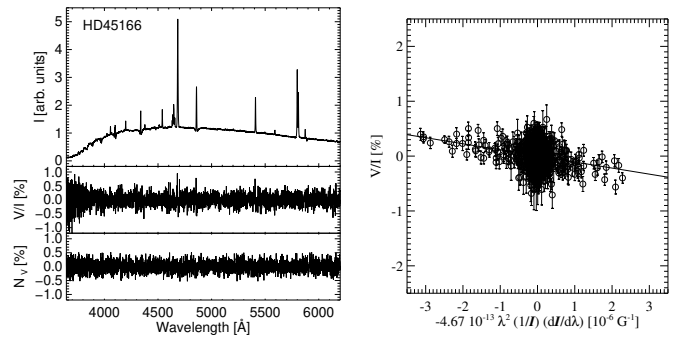


Fig. 1. FORS2 observations of the reference magnetic massive star HD 45166. In the left panel, the solid lines show the recorded Stokes I and Stokes V spectra and the diagnostic N_V spectra, from top to bottom. In the right panel, we show the regression detection of the mean longitudinal magnetic field with $\langle B_z \rangle_{\text{all}} = -1107 \pm 80$ G.

beams, respectively. To allow quality checks, diagnostic null profiles (N_V) were computed as pairwise differences from all available V spectra, which caused the real polarisation signal to be cancelled out. More details on our measurement procedures are presented in numerous previous publications (e.g. Hubrig et al. 2014, 2020; Schöller et al. 2017).

For the determination of the stellar mean longitudinal magnetic field, we usually considered two sets of spectral lines: (i) the entire spectrum that includes all available absorption and emission lines and (ii) exclusively hydrogen lines. For massive stars we always assume a Landé factor $g_{\text{eff}} = 1.0$ for the hydrogen lines and $g_{\text{eff}} = 1.2$ for all other lines. Notably, in our regression analysis we did not differentiate between absorption and emission lines, since the relation between the Stokes V signal and the slope of the spectral line wing (unlike with high-resolution spectropolarimetric observations) holds for both type of lines, so the signals of emission and absorption lines add up rather than cancel out.

The $\langle B_z \rangle$ is defined by the slope of the weighted linear regression line through the measured data points, where the weight of each data point is given by the squared S/N of the Stokes V spectrum. For the magnetic field determination, we used both the spectra extracted using the MIDAS pipeline and those from the IRAF procedures. As the measured magnetic field strengths and measurement accuracies are similar for the two reductions, we took the average of the two values as the final field strength. Linear regression plots for each observed target are presented in Figs. 1–7. The formal 1σ error of $\langle B_z \rangle$ was obtained from

¹ <https://iraf.noirlab.edu/>

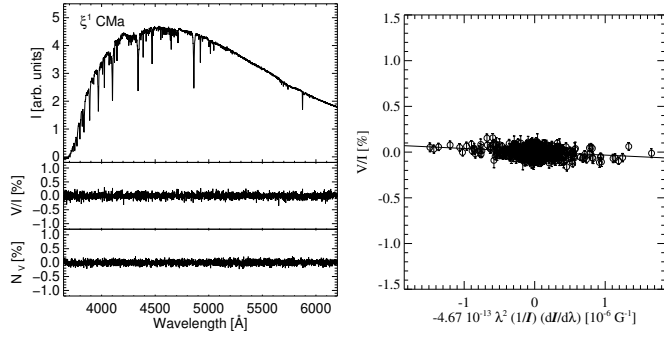


Fig. 2. Same as Fig. 1 but for the reference magnetic massive star ξ^1 CMa, with $\langle B_z \rangle_{\text{all}} = -362 \pm 44$ G.

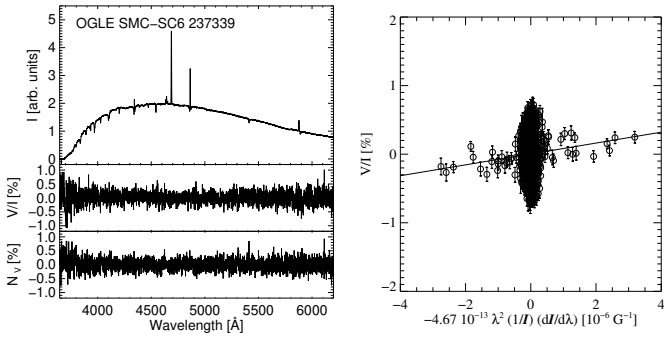


Fig. 3. Same as Fig. 1 but for the Of?p star OGLE SMC-SC6 237339, with a longitudinal magnetic field of $\langle B_z \rangle_{\text{all}} = 794 \pm 209$ G detected at a 3.8σ significance level.

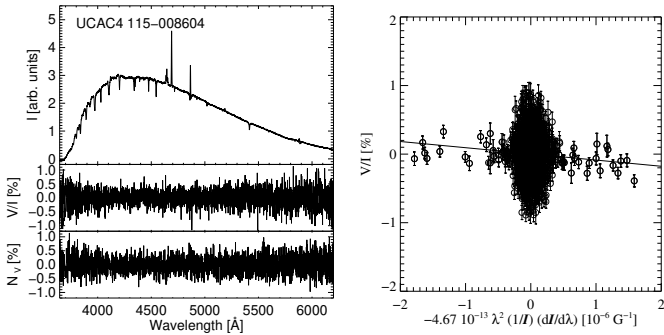


Fig. 4. Same as Fig. 1 but for the Of?p star UCAC4 115-008604 with a longitudinal magnetic field of $\langle B_z \rangle_{\text{all}} = -902 \pm 271$ G detected at a 3.3σ significance level.

the standard relations for weighted linear regression. This error is inversely proportional to the Stokes V rms S/N . Furthermore, to derive robust estimates of standard errors (Steffen et al. 2014; Schöller et al. 2017), we carried out Monte Carlo bootstrapping tests. The measurement uncertainties obtained before and after the Monte Carlo bootstrapping tests were found to be in close agreement, indicating the absence of reduction flaws.

The results of our longitudinal magnetic field measurements, those for the entire spectrum or only the hydrogen lines, are presented in Table 2. We also list the corresponding known rotation periods, the orbital period for SSN 7 – for which the rotation periods of both components are unknown – and the rotation phases at the time of observation. The phases for the Of?p stars were calculated according to the respective periods and ephemerides provided in previous studies (Nazé et al. 2015;

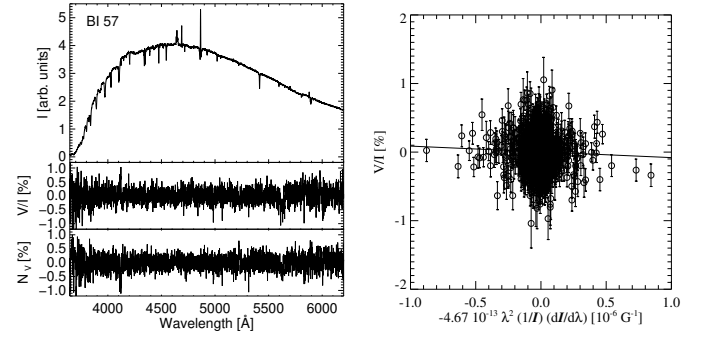


Fig. 5. Same as Fig. 1 but for the Of?p star BI 57, with a mean longitudinal magnetic field measured at a low significance: $\langle B_z \rangle_{\text{all}} = -837 \pm 440$ G.

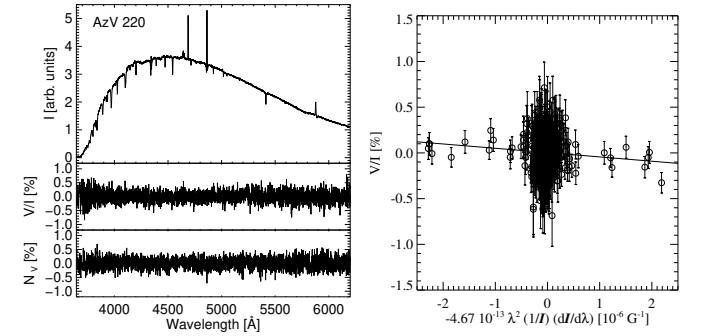


Fig. 6. Same as Fig. 1 but for the Of?p star AzV 220, with a mean longitudinal magnetic field measured at a low significance: $\langle B_z \rangle_{\text{all}} = -472 \pm 202$ G.

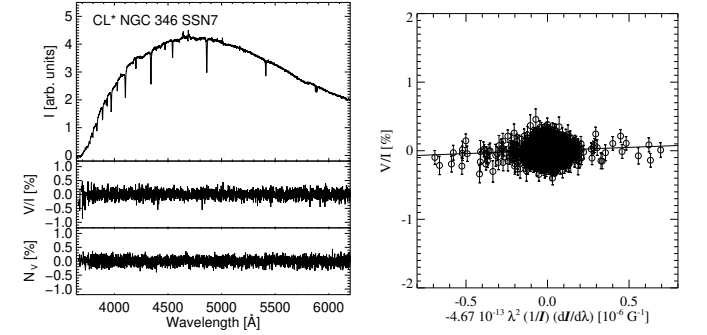


Fig. 7. Same as Fig. 1 but for the contact binary CL* NGC 346 SSN 7, with a mean longitudinal magnetic field of $\langle B_z \rangle_{\text{all}} = 908 \pm 206$ G detected at a 4.4σ significance level.

Bagnulo et al. 2020) using OGLE light curves, with $\phi = 0$ corresponding to the photometric minima.

4. Discussion

In Figs. 1 and 2 we present the observed Stokes I and V spectra, the diagnostic N_V spectra, and the corresponding weighted linear regression lines through the measured data points for the reference magnetic massive stars HD 45166 and ξ^1 CMa. Similar plots for the Of?p stars OGLE SMC-SC6 237339 and UCAC4 115-008604, both of which have detected magnetic fields, are shown in Figs. 3 and 4, and in Figs. 5 and 6 we present the plots for the two Of?p stars with no magnetic field detection, BI 57 and AzV 220. Plots for the contact binary with a detected magnetic field, SSN 7, are shown in Fig. 7. The

Table 2. Results of our magnetic field measurements.

Object	$\langle B_z \rangle_{\text{all}}$ [G]	σ_{all}	$\langle B_z \rangle_{\text{hyd}}$ [G]	σ_{hyd}	$\langle B_z \rangle_{\text{N}}$ [G]	P_{rot}	P_{orb}	Ref.	Phase
OGLE SMC-SC6 237339	794 ± 209	3.8	843 ± 253	3.3	-62 ± 224	1370 d		1	0.545
BI 57	-837 ± 440	1.9	-190 ± 498	0.4	363 ± 452	787 d		1	0.250
AzV 220	-472 ± 202	2.3	-531 ± 262	2.0	109 ± 199	>16 yr		1	
UCAC4 115-008604	-902 ± 271	3.3	-1013 ± 401	2.5	118 ± 282	18.706 d		2	0.296
CI* NGC 346 SSN 7	908 ± 206	4.4	801 ± 274	2.9	-122 ± 216		3.07359 d	3	0.348
ξ^1 CMa	-362 ± 44	8.3	-369 ± 76	4.8	96 ± 42	~ 30 yr		4	
HD 45166	-1107 ± 80	13.8	-1452 ± 254	5.7	-36 ± 76	124.8 d		5	

Notes. The first column lists the object name, followed by the measurement of the longitudinal magnetic field using the full spectrum (Col. 2) and only the hydrogen lines (Col. 4), with the corresponding σ significance of the measurement given in Cols. 3 and 5. Col. 6 lists the measurements carried out using the null spectrum. In Col. 7 we present the rotation period (P_{rot}) for each object and in Col. 8 the orbital period (P_{orb}), with the corresponding reference in Col. 9 ((1) Nazé et al. 2015; (2) Bagnulo et al. 2020; (3) Rickard & Pauli 2023; (4) Erba et al. 2021; (5) Shenar et al. 2023). The rotation or orbital phase for each measurement is listed in Col. 10.

longitudinal magnetic field $\langle B_z \rangle_{\text{all}} = -362 \pm 44$ G measured for our reference target ξ^1 CMa, which has an extremely long rotation period of about 30 yr, is in full agreement with the expected negative extremum of the field predicted to occur in 2024 (Erba et al. 2021). The measurement of HD 45166, reported to possess an extraordinary longitudinal magnetic field of 13.5 kG (Shenar et al. 2023), now shows, for the first time, a negative longitudinal kilogauss-scale field. For this system, the stripped, helium-strong, quasi-Wolf–Rayet component may be due to multiple interactions and a merging event.

Of the four observed Of?p stars, the presence of a mean longitudinal magnetic field, $\langle B_z \rangle_{\text{all}}$, is only detected in OGLE SMC-SC6 237339 (in the SMC), at a significance level of 3.8σ , and in UCAC4 115-008604 (in the LMC), at a significance level of 3.3σ . Minimum dipole strengths (B_d) of 2.4 kG and 2.7 kG were estimated for these two stars using the relation $B_d \geq 3|\langle B_z \rangle_{\text{all}}|$ (Babcock 1958). A longitudinal magnetic field of $\langle B_z \rangle_{\text{all}} = 908 \pm 206$ G at a significance level of 4.4σ is detected in the contact binary system SSN 7. The corresponding minimum B_d value for this system is 2.7 kG. Considering the spectral line content and the radial velocities observed in our FORS2 spectrum of SSN 7, we conclude that the magnetic field is located in the primary component. Due to the very weak contribution of the secondary to the composite spectrum, no conclusion can be drawn about the magnetic nature of this component. As the orbital and stellar parameters for this binary are already known (Rickard & Pauli 2023), we were able to calculate the configuration and orientation of this system at the time of the FORS2 observations using the PHOEBE code (PHysics Of Eclipsing BinariEs²), which is an open source modelling code for computing theoretical light and radial velocity curves (Prša et al. 2016). It is a Wilson-Devinney-like eclipsing binary light curve modelling code that uses Roche geometry to model stellar surfaces. The obtained PHOEBE surface mesh model is presented in Fig. 8.

With regard to the significance levels of 3.8σ and 3.3σ for the magnetic field detections in the Of?p stars OGLE SMC-SC6 237339 and UCAC4 115-008604, we note that the two clearly magnetic Galactic Of?p stars HD 148937 and CPD-28° 2561 were for the first time detected as magnetic in FORS1 and FORS2 observations, at significance levels of 3.1σ and 3.2σ , respectively, using the same instrumental setup

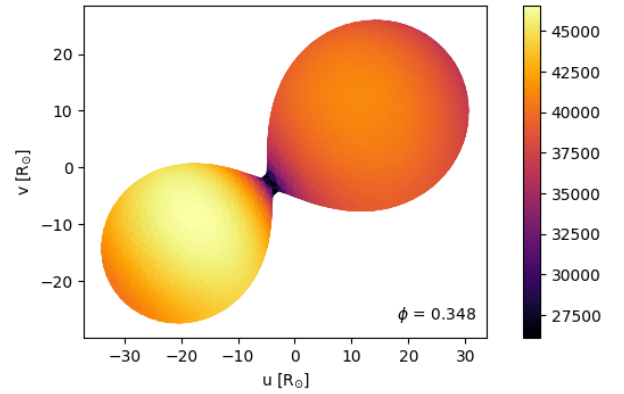


Fig. 8. PHOEBE surface mesh model showing the configuration and plane-of-sky orientation of SSN 7 during the recently obtained FORS2 observations, based on the previously reported orbital solution (Rickard & Pauli 2023). The face colour represents the temperature across the surface (see the colour bar), and the axes show the U and V plane-of-sky orientation in units of solar radius.

(Hubrig et al. 2008, 2011). This indicates that both Of?p stars in the MCs very likely possess kilogauss-scale magnetic fields.

The detection of magnetic fields in Of?p stars – suggested to be merger products in Galactic Of?p stars (Frost et al. 2021) – was more or less expected but was probably hampered by the faintness of the targets. Several years ago, Bagnulo et al. (2017, 2020) carried out similar FORS2 observations, but in different rotation phases and with a different instrumental setup, using GRISM 1200B, a slit width of $1''$, and a binning of 2, therefore covering the wavelength region 3700–5120 Å. In contrast, our instrumental setup using GRISM 600B allowed us to cover a larger wavelength range, from 3250 to 6215 Å, and allowed us to measure a polarisation signal in additional He I, He II, and metal lines, improving the measurement accuracy. Furthermore, only absorption lines were used for the magnetic field measurements by Bagnulo et al. (2017, 2020) despite the fact that Of?p stars present numerous lines that are in emission or display P Cyg-type profiles. None of the obtained measurements of the mean longitudinal magnetic field in that study showed a definite 3σ detection.

The measurement accuracies achieved by Bagnulo et al. (2017, 2020) were of the order of several hundred gauss: 575 G and 305 G respectively for the two observations of AzV 220

² <http://phoebe-project.org>

in 2015 and 2017, compared to our measurement accuracy of 202 G; 530 G for the single observation of OGLE SMC-SC6 237339 in 2015 compared to our accuracy of 209 G; 345 G for the single observation of BI 57 in 2016 compared to our accuracy of 440 G; and 235 G and 275 G for the two observations of UCAC4 115-008604 in 2017 compared to our accuracy of 271 G.

It is not clear whether the non-detections reported by Bagnulo et al. (2017, 2020) were due to the observations being carried out at unfavourable rotational phases. As we report in Sect. 2, because the longitudinal magnetic field is strongly dependent on the viewing angle of the observer (i.e. on the rotation angle of the star), we tried to avoid rotation phases when the light curves for the studied targets were at a minimum. Our observations that yielded field detections were carried out at very different rotational phases than those covered by Bagnulo et al. (2017, 2020). This applies for our observations of OGLE SMC-SC6 237339 at a rotation phase of 0.545 (close to the maximum of the OGLE light curve phase of 0.5), whereas the observations by Bagnulo et al. (2017, 2020) took place at a rotational phase of 0.42. We observed the target UCAC4 115-008604 at a rotational phase of 0.296, which is close to the light curve maximum (~ 0.4), whereas the two previous observations of this target were carried out at rotational phases of 0.74 and 0.85, respectively. Also, our observations of the other two Of?p stars, AzV 220 and BI 57, that yielded non-detections were carried out at different rotational phases than those by Bagnulo et al. (2017, 2020), and they yield very different longitudinal magnetic field strengths. It is possible that the differences between the different field measurements are caused by rotational modulation, but the number of measurements is currently too small to draw any firm conclusion.

The detection of a magnetic field in the extragalactic contact binary SSN 7 in a lower-metallicity environment provides an important constraint on the strength of magnetic fields formed through mass transfer. This detection also allowed us to robustly test theoretical predictions. According to recent numerical simulations (e.g. Schneider et al. 2019), the magnetic field is formed in two steps, first when the binary system begins its mass transfer and second when the cores of the two components come into contact. In the first step, shear between the accreting stream and the surface of the accretor forms a modest magnetic field, which is then bolstered considerably during the second step when the cores merge. Therefore, magnetic fields in massive stars would only be expected in actively interacting or post-interaction systems. Importantly, stripped-envelope stars formed in systems with interacting components through one or multiple phases of Roche-lobe overflow may be the progenitors of gravitational waves (e.g. Laplace et al. 2020). It is of interest that rather strong longitudinal magnetic fields have recently been reported for the two well-known Galactic over-contact binaries LY Aur (= HD 35921) and MY Ser (= HD 167971) by Hubrig et al. (2023). Together with Plaskett’s star – which is in a semi-detached configuration (Grunhut et al. 2022) – these are the only known Galactic magnetic O-type stars in close binary systems that fit the proposed scenario, as the over-contact phase is the last evolutionary phase before a massive stellar merger.

It is not clear whether studies of pulsations can help discriminate between magnetic and non-magnetic pulsating massive stars. A recent study by Kurtz et al. (2020) reported the detection of coherent pulsation modes in the Of?p star NGC 1624-2 based on high-cadence Transiting Exoplanet Survey Satellite (TESS; Ricker et al. 2015) photometry. With a surface magnetic field strength of the order of 12 kG, this star possesses the strongest magnetic field ever measured in an O-type star (e.g.

Järvinen et al. 2021). For all targets in our sample, TESS data are available, although a careful analysis is necessary because the signal can be affected by contamination from nearby stars in the crowded field of view. Interestingly, our preliminary inspection of TESS data indicates the possible presence of periods of several hours to one day in three Of?p stars, but does not confirm the previously reported 18.7 d rotation period for UCAC4 115-008604 (Bagnulo et al. 2020) or the spectroscopic period of about 3 d for SSN 7 (Rickard & Pauli 2023).

Studies of magnetic fields in massive stars with lower metallicities provide important information on the role of magnetic fields in star formation in the early Universe in minimally polluted gas. Our magnetic field detections in two Of?p stars and one contact binary located in the MCs suggests that the impact of the lower-metallicity environment of the MCs on the occurrence and strength of stellar magnetic fields in massive stars is low. However, because the explored stellar sample is very small, additional observations of massive stars in the MCs are needed. Notably, studies of other characteristics of massive stars in these galaxies report that lower metallicities lead to a lower opacity of the lines that drive the wind, which has an important effect on the wind characteristics of a star (i.e. the terminal velocity and the mass-loss rate; Vink et al. 2001). The modified mass loss, however, impacts the evolution, rotation, nucleosynthesis, and ionising photon production of massive stars. While the physical properties of the Of?p stars in our sample have not yet been studied in detail, the spectroscopic and orbital characteristics of the contact system SSN 7, including the evolutionary model, are already available thanks to its location in a frequently surveyed starburst region of the SMC. It has been suggested that SSN 7 is the most massive Algol-like system discovered to date (Rickard & Pauli 2023). The mass of the primary component, $M_1 = 32 M_\odot$, is surprisingly low for its luminosity, and the mass of the secondary is $M_2 = 55 M_\odot$. The low mass of the primary indicates that the binary components must be interacting or have interacted in the past. Indeed, their Roche radii suggest that the stars are still in contact, currently slightly overflowing their Roche lobe with $R_1/R_{RL} = 1.01$ and $R_2/R_{RL} = 1.03$. A characterisation of the targets with detected magnetic fields – including their atmospheric parameters, wind properties, and magnetic field geometry – is urgently needed to anchor stellar models appropriate for a lower-metallicity environment.

Acknowledgements. We thank the anonymous referee for constructive comments and suggestions. Based on observations collected at the European Southern Observatory under ESO programme 111.24JY.001. This Letter includes data collected by the TESS mission. Funding for the TESS mission is provided by the NASA’s Science Mission Directorate. NOIRLab IRAF is distributed by the Community Science and Data Center at NSF NOIRLab, which is managed by the Association of Universities for Research in Astronomy (AURA) under a cooperative agreement with the U.S. National Science Foundation. This project received the support of two fellowships from “La Caixa” Foundation (ID 100010434). The fellowship codes are LCF/BQ/PI23/11970031 (AE) and LCF/BQ/PI23/11970035 (MAM). The authors would like to thank the Paranal team for the excellent support during the execution of the programme.

References

- Angel, J. R. P., & Landstreet, J. D. 1970, *ApJ*, **160**, L147
 Appenzeller, I., Fricke, K., Fürtig, W., et al. 1998, *Messenger*, **94**, 1
 Babcock, H. W. 1958, *ApJS*, **3**, 141
 Bagnulo, S., Nazé, Y., Howarth, I. D., et al. 2017, *A&A*, **601**, A136
 Bagnulo, S., Wade, G. A., Nazé, Y., et al. 2020, *A&A*, **635**, A163
 Cikota, A., Patat, F., Cikota, S., & Faran, T. 2017, *MNRAS*, **464**, 4146
 Dufton, P. L., Evans, C. J., Hunter, I., Lennon, D. J., & Schneider, F. R. N. 2019, *A&A*, **626**, A50

- Ekström, S., Meynet, G., Georgy, C., et al. 2019, in Dwarf Galaxies: From the Deep Universe to the Present, eds. K. B. W. McQuinn, & S. Stierwalt, *International Astronomical Union Symposia*, 344, 153
- Erba, C., Shultz, M. E., Petit, V., et al. 2021, *MNRAS*, 506, 2296
- Frost, A. J., Mahy, L., Sana, H., et al. 2021, *OBA Stars: Variability and Magnetic Fields*, 19
- Grunhut, J. H., Wade, G. A., Neiner, C., et al. 2017, *MNRAS*, 465, 2432
- Grunhut, J. H., Wade, G. A., Folsom, C. P., et al. 2022, *MNRAS*, 512, 1944
- Hubrig, S., Kurtz, D. W., Bagnulo, S., et al. 2004a, *A&A*, 415, 661
- Hubrig, S., Szeifert, T., Schöller, M., Mathys, G., & Kurtz, D. W. 2004b, *A&A*, 415, 685
- Hubrig, S., Briquet, M., Schöller, M., et al. 2006, *MNRAS*, 369, L61
- Hubrig, S., Schöller, M., Schnerr, R. S., et al. 2008, *A&A*, 490, 793
- Hubrig, S., Schöller, M., Kharchenko, N. V., et al. 2011, *A&A*, 528, A151
- Hubrig, S., Schöller, M., & Kholtygin, A. F. 2014, *MNRAS*, 440, 1779
- Hubrig, S., Schöller, M., Cikota, A., & Järvinen, S. P. 2020, *MNRAS*, 499, L116
- Hubrig, S., Järvinen, S. P., Ilyin, I., Schöller, M., & Jayaraman, R. 2023, *MNRAS*, 521, 6228
- Järvinen, S. P., Hubrig, S., Schöller, M., et al. 2021, *MNRAS*, 501, 4534
- Kurtz, D. W., Hubrig, S., Järvinen, S. P., & Schöller, M. 2020, *Res. Notes Am. Astron. Soc.*, 4, 157
- Laplace, E., Göteborg, Y., de Mink, S. E., Justham, S., & Farmer, R. 2020, *A&A*, 637, A6
- Munoz, M. S., Wade, G. A., Nazé, Y., et al. 2020, *MNRAS*, 492, 1199
- Nazé, Y., Walborn, N. R., Morrell, N., Wade, G. A., & Szymański, M. K. 2015, *A&A*, 577, A107
- Neugent, K. F., Massey, P., & Morrell, N. 2018, *ApJ*, 863, 181
- Pelisoli, I., Dorsch, M., Heber, U., et al. 2022, *MNRAS*, 515, 2496
- Prša, A., Conroy, K. E., Horvat, M., et al. 2016, *ApJS*, 227, 29
- Regimbau, T., & de Freitas Pacheco, J. A. 2006, *A&A*, 447, 1
- Rickard, M. J., & Pauli, D. 2023, *A&A*, 674, A56
- Ricker, G. R., Winn, J. N., Vanderspek, R., et al. 2015, *J. Astron. Telesc. Instrum. Syst.*, 1, 014003
- Schneider, F. R. N., Podsiadlowski, P., Langer, N., Castro, N., & Fossati, L. 2016, *MNRAS*, 457, 2355
- Schneider, F. R. N., Ohlmann, S. T., Podsiadlowski, P., et al. 2019, *Nature*, 574, 211
- Schneider, F. R. N., Ohlmann, S. T., Podsiadlowski, P., et al. 2020, *MNRAS*, 495, 2796
- Schöller, M., Hubrig, S., Fossati, L., et al. 2017, *A&A*, 599, A66
- Shenar, T., Wade, G. A., Marchant, P., et al. 2023, *Science*, 381, 761
- Steffen, M., Hubrig, S., Todt, H., et al. 2014, *A&A*, 570, A88
- Tody, D. 1993, in *Astronomical Data Analysis Software and Systems II*, eds. R. J. Hanisch, R. J. V. Brissenden, & J. Barnes, *ASP Conf. Ser.*, 52, 173
- Uzdensky, D. A., & MacFadyen, A. I. 2006, *ApJ*, 647, 1192
- van Dokkum, P. G. 2001, *PASP*, 113, 1420
- Vink, J. S., de Koter, A., & Lamers, H. J. G. L. M. 2001, *A&A*, 369, 574
- Walborn, N. R. 1972, *AJ*, 77, 312
- Walborn, N. R., Sota, A., Maíz Apellániz, J., et al. 2010, *ApJ*, 711, L143
- Walborn, N. R., Morrell, N. I., Nazé, Y., et al. 2015, *AJ*, 150, 99